Modeling Atomic and Molecular Plasma Processes During Startup of PFRC-2

Grant Rutherford
*Brown University**

Eugene S. Evans and Samuel A. Cohen
Princeton Plasma Physics Lab
(Dated: September 22, 2020)

To study how initial conditions of PFRC-2, a reversed-field configuration device at Princeton, affect startup and the relative importance of different processes during startup, we constructed and solved a 0D model as an initial value problem. Incorporated into the model are hydrogen processes using collisional radiative rate coefficients taken from EIRENE, charged particle loss due to flow parallel to B, enhanced confinement from mirror fields and the FRC, electron interactions with the ends of the machine, and subsequent generation of nonthermal, high energy electrons. By solving the model we obtain electron density and energy as a function of time and can determine the delay to densification. Additionally, we present trends in these outputs as functions of major machine inputs, namely: P_{in}, n_{H_2}, τ_e and B.

I. INTRODUCTION

A. PFRC-2

PFRC-2 (Princeton Field Reversed Configuration) is the second in a series of four devices that will determine the feasibility of a novel, high-β, compact reactor design. This design uses an odd-parity rotating magnetic field (RMF) to form and heat an FRC by driving an azimuthal plasma current. Such a design has applications as a small, aneutronic fusion (D-^{3}He) reactor and as a rocket engine.

PFRC-2 is composed of three segments: the source end cell, central cell, and far end cell. Between each segment are mirror coils, shown in pink in Fig 1, that produce a mirror field in addition to the axial field produced by the axial field coils (shown in green). Our model focuses entirely on the central cell as this is where the RMF interacts with the plasma, where the FRC is produced, and where the fusion reactions would take place.

A notable phenomenon in PFRC-2 is the presence of a high energy electron population[1]. These electrons are generated via secondary electron emission when protons impact the end plates in the source end cell and far end cell. These plates have changing potentials during operation and can become highly negative. If electrons are emitted when this is the case, those electrons will be accelerated to several keV, forming a population of electrons far more energetic than the bulk electrons.

B. Startup of PFRC-2

Startup of PFRC-2 begins in the source end cell where a helicon antenna ionizes the gas in the chamber and forms a low density ($n_e \approx 10^9$ cm^{-3}) seed plasma. This seed plasma is transported to the central cell, and the RMF is turned on. The purpose of the seed plasma is to give the RMF something to couple to, which increases the consistency of startup[2]. The process of transitioning from the seed plasma to the higher density ($n_e \approx 10^{13}$ cm^{-3}) final plasma is known as densification and is the part of startup our model investigates. Therefore our model begins with the seed plasma already in place in the central cell.

II. THE MODEL

A. How It Works

Our model works by keeping track of the number density, n_s, and total energy, E_s, of each species of interest. Those species are: low energy electrons, high energy electrons, protons, atomic hydrogen, molecular hydrogen, and molecular ions. Together with ODEs for n_s and E_s and some initial values, we can evolve them though time using SciPy's solve_ivp method.

B. Goals

The goal of the model is to aid us in better understanding the general behavior of the plasma as densification occurs, the effect of initial conditions on densification, the relative importance of different processes, and what role the high energy electrons play in startup.

C. Model Simplifications

Due to the complexity of startup and the limited time frame of the summer, a number of simplifications were made. The most important of these is that the model is a 0D model, so there is no spatial component. Because of

* grant_rutherford@brown.edu

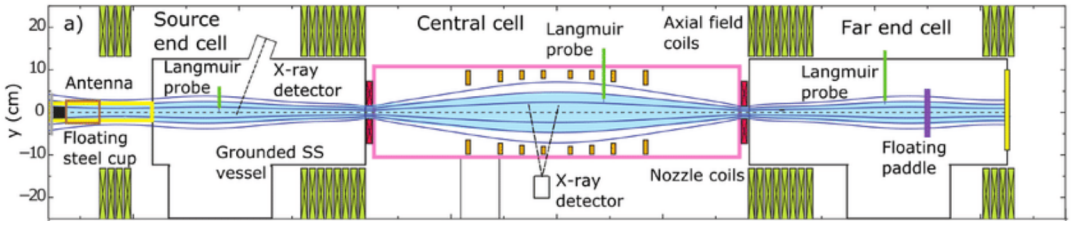

FIG. 1: Schematic of PFRC-2

this, we cannot directly model the FRC. Instead we must use free parameters to incorporate the affects of the FRC. Similarly, we cannot generate spatial gradients.

Other simplifications include excited states being wrapped into rate coefficients generated by a collisional radiative model obtained from the EIRENE code's atomic/molecular physics database, assuming the magnetic moment is adiabatic for mirror trapped particles, assuming that all distributions are Maxwellian, assuming the plasma is cylindrical in shape, and having no delay between a particle leaving the plasma via Bohm diffusion and either scattering back into the plasma or returning as a recycled neutral.

Additionally, we do not allow the temperature of the high energy electron population to vary. Experimentally, we find they do not stick around long enough for their temperature to change appreciably.

D. Processes in the Model

Included in the model are many processes. Those that take place between particles and modify the number densities are listed in Table I, and all other major processes are listed in Table II.

There are multitude of free variables in the model, several of which have far-reaching effects. We will now go through some selected processes and discuss both their implementation and the free variables associated with them.

Process:	**Reaction:**
Ionization	$e + H \rightarrow 2e + H^+$ $H_2 + e^- \rightarrow H_2^+ + 2e$
Dissociative ionization	$H_2 + e \rightarrow H + H^+ + 2e$ $H_2^+ + e \rightarrow 2H^+ + 2e$
Recombination	$H^+ + e \rightarrow H$
Dissociative recombination	$H_2^+ + e \rightarrow 2\mathrm{H}$
Dissociation	$H_2 + e \rightarrow 2H + e$ $H_2^+ + e \rightarrow H + H^+ + e$
Charge exchange	$H_2 + H^+ \leftrightarrow H_2^+ + H$ $H + H^+ \rightarrow H^+ + H$

TABLE I: List of the inter-particle processes that modify number density

Process:
Axial losses, reduced by mirror effects
Bohm losses
Bremsstrahlung losses
H_2 gas puffs
Recycling and elastic collisions with the chamber
Restorative influx of H_2 gas
Thermalization

TABLE II: Additional processes

1. *Recycling*

Ions lost via Bohm diffusion are given a 50% chance of recycling when they collide with the chamber wall. Protons have equal probabilities of recombining as H or H_2 while molecular ions will only recombine into H_2. Also, atomic hydrogen colliding with the wall is equally likely to form H_2 as it is to elastically scatter.

Newly-formed H particles are returned to the plasma with an energy of 0.5 eV whereas newly-formed H_2 particles are given an energy of 0.038 eV $= \frac{3}{2}T_{room}$. This lower energy is due to the lengthier process of forming an H_2 particle, which gives them adequate time to thermalize with the room-temperature wall.

Particles that scatter off of the wall instead of recombining have their energy reduced according to

$$\delta E = \frac{3}{2} \cdot (T_{room} - T_s) \cdot \alpha_{loss,coll}, \tag{1}$$

where s is the species and $\alpha_{loss,coll}$ is a free parameter currently set to $\frac{1}{2}$.

2. *Restorative Influx vs Gas Puffs*

While both the restorative influx and gas puffs provide additional H_2 to the central cell and thus to the plasma, they do so in different ways. The restorative influx attempts to restore n_{H_2} to its initial value. Since we are operating in a mostly collisionless regime, the plasma does not significantly affect the equilibrium of the gas, and thus the H_2 gas outside of the plasma seeks to reestablish the initial H_2 number density $n_{H_{2_0}}$ inside the plasma. The equation for this flux is

$$\Gamma_{restor} = (n_{H_{2_0}} - n_{H_2}) \cdot v_{th} \cdot \frac{r_{\text{plasma}}}{Area_{\text{plasma}}} \tag{2}$$

Gas puffs on the other hands are simply large influxes of H_2. Currently PFRC-2 does not operate with gas puffs during startup, but we are interested in seeing what effect it may have. When we allow gas puffs to occur in the simulation, we have chosen to trigger a puff when the total electron number density $n_e = n_{eLow} + n_{eHigh} < 5 \cdot 10^{12}$ cm^{-3}.

Puffs have a minimum length of 100 μs and a maximum length of 300 μs with at least 150 μs between puffs. Additionally, there is a 50 μs delay between the trigger and gas reaching the plasma. Likewise, once a puff is stopped, it takes 50 μs for gas to stop entering the plasma. The puff rate was chosen semi-arbitrarily to be $5 \cdot 10^{16}$ cm$^{-3}s^{-1}$.

3. *Axial Losses*

Particles in the central cell are constantly being lost as they spiral around the magnetic field lines and flow into the other sections. Since electrons are lost much more rapidly than the ions, the plasma develops potentials in order to maintain quasineutrality. The ion sound speed c_s then becomes the speed of lost particles. Using that velocity together with a length scale ℓ_{plasma}, which we have chosen to be half the length of the plasma, we can define an approximate loss rate

$$\Gamma_{axial\ loss} = \frac{c_s}{\ell_{plasma}} \tag{3}$$

However, there is also the affect of the mirror field; some portion of particles that would be lost are instead returned to the plasma. Assuming the magnetic moment of particles is adiabatic, a mirror ratio M of 5, and $T_\perp = T_\parallel$, we find that 10.6% of particles are not reflected by the mirror and escape.

Additionally, some confinement is provided by the FRC, which we incorporate via a reducing factor, $r_{reducing}$. Note that a smaller reducing factor provides greater confinement. We typically set $r_{reducing} = 0.25$. Our final loss term is then

$$\Gamma_{axial\ loss} = \frac{r_{reducing} \cdot m_{escape} \cdot c_s}{\ell_{plasma}} \tag{4}$$

4. *Helicon and RMF heating*

The helicon antenna that produces the seed plasma also provides a constant source of power for the plasma throughout densification given by

$$P_{\text{eff, helicon}} = \frac{1.6W}{V_{\text{helicon plasma}}} \tag{5}$$

The volume specified here is not the plasma volume but is instead the volume of plasma stretching from the antenna throughout the central cell (2 meters long, ~6 cm in radius). Comparing this term and the RMF power described below, the helicon power is seen to be insignificant once RMF turns on. However, prior to RMF, this term is highly important for maintaining steady state.

RMF heating is an integral part of PFRC-2's operation, and it is important that we are modeling it reasonably well. That being said, we use a highly simplified model of plasma-RMF coupling due to the exact dynamics not being well understood. Using 20 kW as an approximate value for the maximum power the whole plasma can absorb and assuming that the absorbed power both scales with n_e and saturates close to $n_e = 5 \cdot 10^{12}$ cm^{-3}, we have

$$P_{\text{eff, RMF}} = \frac{20kW \cdot \min(\frac{n_e}{5 \cdot 10^{12}}, 1)}{V_{\text{plasma}}} \tag{6}$$

5. *Changing Radius*

Experimentally, we find that there are two timescales to densification, a slow timescale and a fast timescale, seen in Fig 2 (Note that the RMF input powers listed are the forward powers whereas the RMF power that we use in the model is the effective absorbed power and is thus substantially smaller). Though the exact cause of this behavior is unknown, one hypothesis is that the plasma radius shrinks due to increased confinement from the burgeoning FRC.

Our model seeks to investigate this hypothesis, and we do so by initiating a radius change when the low energy electron density n_{eLow} reaches 10^{11} cm^{-3}. At that point, the radius changes linearly from 6 cm to 3 cm over the course of 5 μs. Additionally, we decrease the plasma length from 30 cm to 12 cm and the axial confinement increases by a factor of two over those 5 μs.

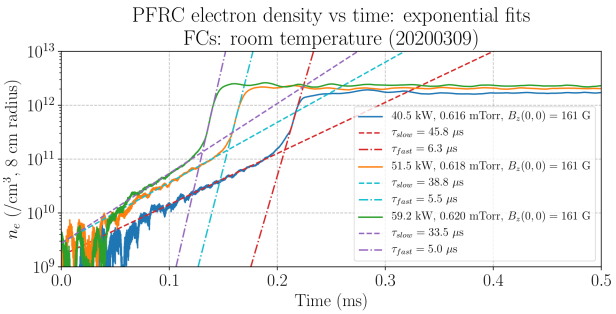

FIG. 2: Experimental runs showing the two timescales of densification

III. RESULTS

A. Working Parameters

Unless stated otherwise, all simulations were run with no gas puffs, an initial fill pressure of 0.5 mTorr $\Rightarrow n_{H_{2_0}} =$

$1.65 \cdot 10^{13}$ cm^{-3}, $B = 200$ G, a max RMF power of 20 kW that turns on at 25 μs, and high energy electrons that are injected with an energy of 750 eV. Additional free parameter values related to some processes are described in the prior section.

B. General Behavior of the Model

Shown in Fig 3 is a simulation run using the parameters described above. Starting at t = 0, we see that the plasma is close to steady state. This is the desired behavior since the seed plasma is in equilibrium before densification. Next, when RMF turns on there is a sharp spike in T_{eLow} before it plateaus as the absorbed RMF power is balanced by the losses from ionization[3] and the addition of newly freed, colder electrons pulling the average temperature down. When n_{eLow} hits 10^{11} cm^{-3} we trigger a radius change, producing a second, faster timescale of densification.

Going back in time slightly to the slow densification region, we find the molecular ions to be substantially more numerous than the protons. As of now we have been unable to find evidence as to whether this is physical or not, and this phenomenon may very well be a quirk of the model.

Once the fast densification region begins, T_{eLow} increases due to the increase in RMF power caused by the decrease in plasma volume. This momentary increase is short lived, and T_{eLow} falls slightly as ionization losses grow too large. But once the ionization rate decreases due to the plasma becoming mostly ionized, T_{eLow} is able to rise once again.

Throughout the simulation, electrons are thermalizing with protons and molecular ions (protons and molecular ions are also thermalizing, but the effect is far less important). Protons and molecular ions also undergo charge exchange with the neutrals, raising T_H and T_{H_2}. One may notice that T_{H_2} is not plotted. This is because that curve is a flat line at room temperature due to the vast amounts of H_2 outside of the plasma that the H_2 in the plasma thermalizes with.

C. Experimental Results

In Fig 4 are simulation runs matching the parameters of the three experimental runs shown in Fig 2. As a careful reader may notice, there are substantial differences between these two plots. Of note is that the three experimental runs are far more similar to each other than the simulated runs are to each other. Given that the pressure barely changes between run, it is thus likely our RMF-plasma coupling is far from correct and that the model is too sensitive to RMF power. Before we fix that issue, it would be difficult to determine if there are other deficiencies the model possesses that keeps it from matching experiments.

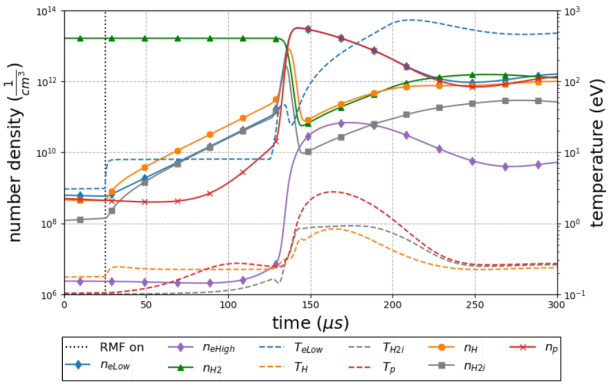

FIG. 3: Example simulation run with our normal operating parameters

D. Effects of High Energy Electrons

The effect of high energy electrons is most readily seen by sweeping over parameters and plotting the difference between simulations with and without high energy electrons of the time at which the radius shrinks – the radius transition time – and of the two timescales.

Beginning with a sweep over $P_{\text{eff RMF}}$ (Fig 5), we find that simulations with the high energy electrons present always had quicker radius transition times than those without, so it would appear that high energy electrons' main affect is to increase the rate of ionization.

The effect of the high energy electrons on the slow timescale and radius transition time is less significant at higher RMF powers since the ionization rate is already being increased by the higher absorbed power, making the high energy electrons' effect less noticeable. The difference in fast timescale does not follow such a trend, instead having minimal differences regardless of presence of high energy electrons up until around 23 kW. Due to the distinct lack of smoothness in the fast timescale curve, it is reasonable to think this effect may be a nonphysical effect.

Next, sweeping over the magnetic field strength (Fig 6), the effect is similar to the RMF case. The slow timescales and radius transition times are always faster with high energy electrons present. This time the fast timescale curve is even more odd. The majority of the fast timescale curve is negative, but given its overall shape, it is hard to make any inferences from it besides that the model likely has some issues. Interestingly, the effect of high energy electrons is more pronounced at higher magnetic fields, where the confinement against Bohm losses is greater.

The final comparison sweep is over the initial fill density (Fig 7) and has notably different behavior than the other two comparison sweeps. Firstly, the fast timescale curve is fairly smooth. But there is a spike near $n_{H_{2_0}} = 1.3 \cdot 10^{13}$ cm^{-3}. Given the overall smoothness of the curve, this has a chance to be physical. Secondly and

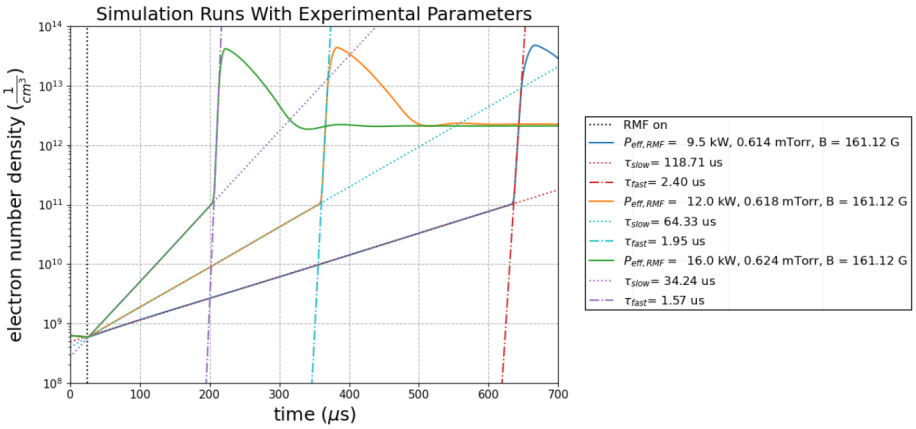

FIG. 4: Simulations with the same parameters as the experimental runs of Fig 2

more importantly, for $n_{H_2{}_0} \lesssim 1.1 \cdot 10^{13}$ cm^{-3}, the simulations without high energy electrons had faster radius transition times. What makes this region special such that it produces the opposite effect is currently unknown and requires further work.

The remainder of the results in this section will be presented with high energy electrons present.

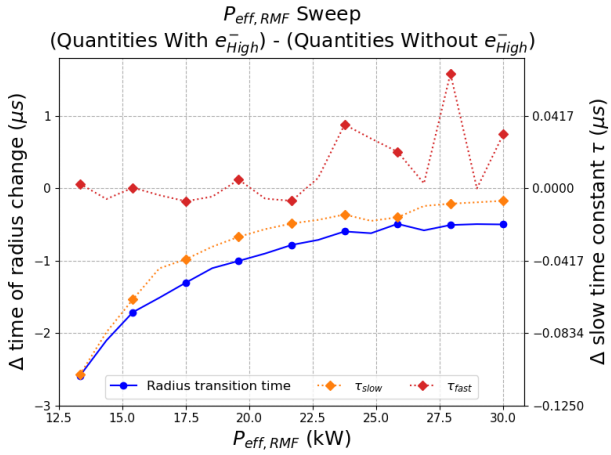

FIG. 5: Differences between timescales and radius transition times with and without high energy electrons, sweeping over $P_{\text{eff RMF}}$

E. Magnetic Field Sweep

Looking to Fig 8, we see that with increasing magnetic field, the radius transition time and both timescales decrease. We believe this to be due to greater confinement against Bohm losses with increasing field strength. A greater confinement means more electrons stay in the plasma, causing the electron cascade to happen more rapidly and thus n_e reaches 10^{11} cm^{-3} more rapidly.

The scaling with B seems to follow some scaled rational function $f(B) = \frac{\gamma}{B}$, which makes sense since the Bohm

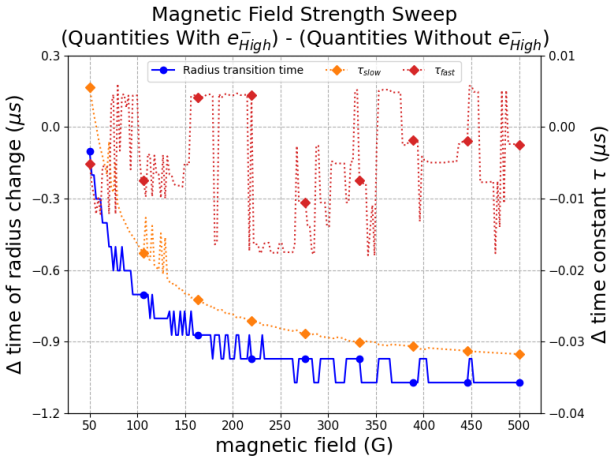

FIG. 6: Differences between timescales and radius transition times with and without high energy electrons, sweeping over magnetic field strength

diffusion coefficient $D_B \propto \frac{k_B T}{eB}$. Therefore D_B varies as a function of B like a rational function, producing the witnessed effect.

F. Initial Fill Density Sweep

In Fig 9, the radius transition time and slow densification timescale are shown to be increasing with increased fill density. However, the fast time scale decreases with increasing fill density. Thus, while it is more difficult to begin ionizing for higher fill densities, once the plasma is sufficiently ionized, it progresses more rapidly.

G. $P_{\text{eff, RMF}}$ Sweep

As is expected, increasing RMF power (Fig 10) decreases both timescales of densification and the radius

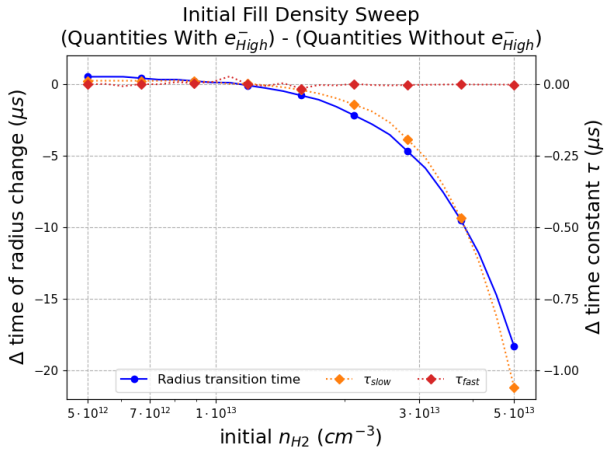

FIG. 7: Differences between timescales and radius transition times with and without high energy electrons, sweeping over initial fill density

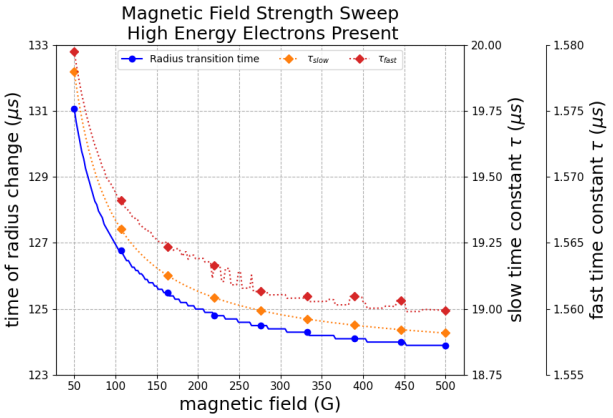

FIG. 8: Parameter sweep over the magnetic field

transition time. This makes sense given that more RMF power means a hotter plasma. And since the peak ionization rate does not occur until $T_e \approx 100$ eV, heating our plasma more during densification will increase the ionization rate.

H. Axial Confinement Sweep

In Fig 11, we sweep over the axial loss reducing factor, r_{reducing}, described in section II D 3. As a reminder, a smaller r_{reducing} produces greater confinement. Again, as in the magnetic field strength sweep, the slow time scale and radius transition time decrease with increased confinement. However, in the magnetic field sweep, the fast timescale decreased fairly smoothly. Here there is far more variation than is expected, though it is perhaps generally trending downward.

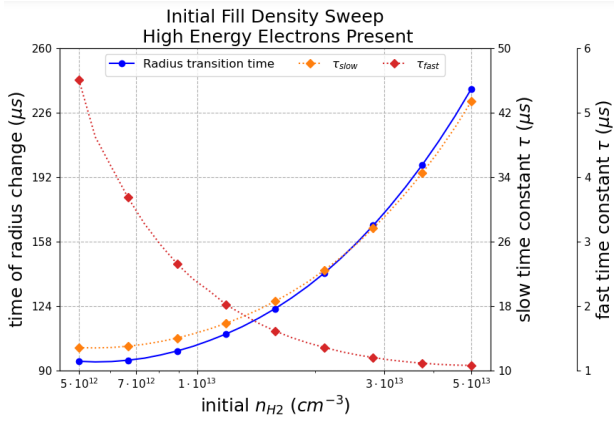

FIG. 9: Parameter sweep over the initial fill density

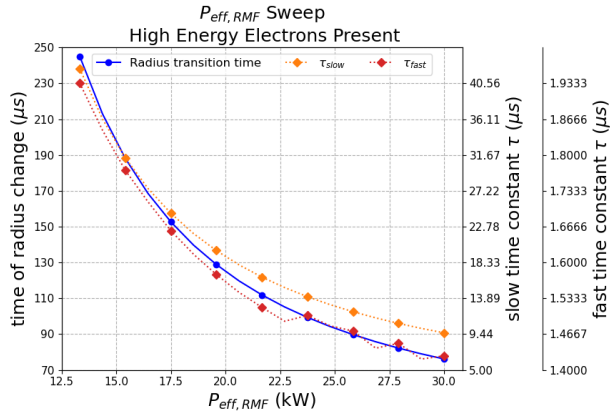

FIG. 10: Parameter sweep over effective RMF power

I. Gas Puffs

According to Fig 12, below a puff rate of around 10^{15} cm^{-3}s^{-1}, gas puffs make little to no difference to the time scales or radius transition time. Above this value, gas puffs lead to a slower slow timescale and thus a slower radius transition time, similar to the effect of increasing fill density. The fast timescale follows a more interesting behavior of at first decreasing but then increasing again for puff rates $\gtrsim 3 \cdot 10^{15}$ cm^{-3}s^{-1}.

IV. CONCLUSION

The model does an exceedingly poor job of quantitatively reproducing experimental results, likely due to overly simplified RMF-plasma dynamics. However, the qualitative behavior of experimental runs are reproduced fairly well.

By comparing the timescales and radius transition times of several parameter sweeps with and without high energy electrons, we found that generally the effect of high energy electrons is to increase the ionization rate. However, there are values of initial fill density where these

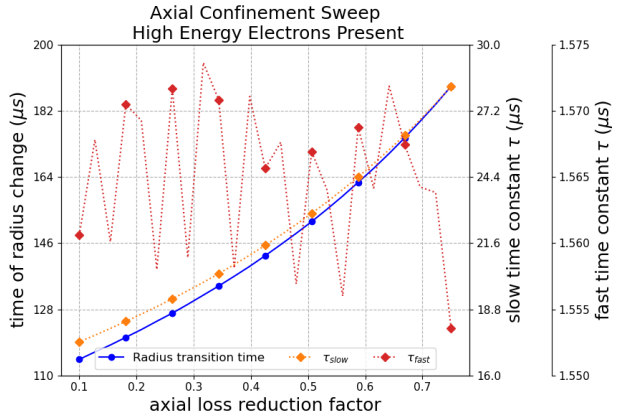

FIG. 11: Parameter sweep over the axial loss reduction factor

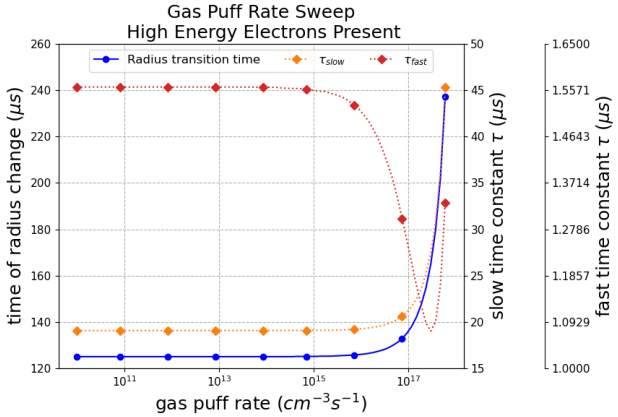

FIG. 12: Parameter sweep over the gas puff rate

particles actually slowed the ionization rate. Why the effect is different for this region is unknown and warrants further study. It is also important to remember that we may be missing major components of the high energy electron dynamics, so these results might differ substantially from experiment.

From the axial loss and magnetic field strength sweeps, densification proceeds more rapidly with greater confinement due to a larger electron population and thus a faster electron cascade. The RMF sweep showed the predicted behavior of faster densification with increasing RMF power.

Increasing fill density leads to a slower slow densification region but a faster fast densification region. Past a certain puff value, gas puffs also lead to a slower slow densification region, but while the fast timescale at first decreases, it increases at large enough puff rates.

Moving forward, we plan to further investigate RMF-plasma coupling and find a less approximate equation for $P_{\text{eff, RMF}}$, add a spatial dimension to better model plasma transport processes, and add nonadiabaticity of μ, which is important to better understanding the high energy electrons[4].

V. ACKNOWLEDGEMENTS

I would like to thank Eugene Evans for answering my many, many questions and for teaching me so much about plasma modeling, the PFRC group for providing great feedback and suggestions, and a huge thank you to Arturo Dominguez and Deedee Ortiz for somehow managing to make a remote internship work well.

This work was made possible by funding from the Department of Energy for the Summer Undergraduate Laboratory Internship (SULI) program. This work is supported by the US DOE Contract No. DE-AC02-09CH11466.

[1] P. Jandovitz, C. Swanson, J. Matteucci, R. Oliver, J. Pearcy, and S. A. Cohen, Demonstration of fast-electron populations in a low-pressure, low-power, magnetized rf plasma source, Physics of Plasmas **25**, 10.1063/1.4998735 (2018), https://doi.org/10.1063/1.4998735.

[2] G. G. Jusino and S. Cohen, A study on the formation of rmf plasma in the pfrc-2, (2019).

[3] R. Janev, D. Post, W. Langer, K. Evans, D. Heifetz, and J. Weisheit, Survey of atomic processes in edge plasmas, Journal of Nuclear Materials **121**, 10 (1984).

[4] C. Swanson, *Measurement And Characterization Of Fast Electron Creation, Trapping, And Acceleration In An Rf-Coupled High-mirror-ratio Magnetic Mirror*, Ph.D. thesis, Princeton University (2018).

[5] M. F. A. Harrison, Atomic and molecular collisions in the plasma boundary, in *Physics of Plasma-Wall Interactions in Controlled Fusion*, edited by D. E. Post and R. Behrisch (Springer US, Boston, MA, 1986) pp. 281–349.

[6] F. Engelmann, Introduction: Approaches to controlled fusion and role of plasma-wall interactions, in *Physics of Plasma-Wall Interactions in Controlled Fusion*, edited by D. E. Post and R. Behrisch (Springer US, Boston, MA, 1986) pp. 15–39.